IJE TRANSACTIONS B: Applications Vol. 34, No. 11, (November 2021) 2379-2386

International Journal of Engineering

Journal Homepage: www.ije.ir

# Design and Optimization of Halbach Permanent Magnet Array with Rectangle Section and Trapezoid Section

N. Song[a], M. Zhu*[a], G. Zhou[a], L. Guo[a], Y. Mu[a], J. Gao[a], J. Ma[a], K. Zhang[b]

[a] *Institute of Automation, Qilu University of Technology (Shandong Academy of Sciences), Shandong Provincial Key Laboratory of Automotive Electronics Technology, Jinan, Shandong, China*

[b] *Rongcheng Rongjia Power Co., LTD, Rongcheng, Shandong, China*

*PAPER INFO*

*Paper history:*
Received 25 April 2021
Received in revised form 21 June 2021
Accepted 29 July 2021

*Keywords*:
*Magnetic*
*Halbach Array*
*Surface Current Method*
*Genetic Algorithm*
*Optimization*

*ABSTRACT*

In this work, a novel Halbach permanent magnet array with rectangle section and trapezoid section is proposed and optimized. The analytical model of the Halbach array is established based on the surface current method, which is numerically efficient and can be utilized to evaluate the magnetic field of the Halbach array caused by varying magnet segment's configurations. The fundamental component of the magnetic flux density and the sinusoidal distortion rate are chosen as the optimization object and the optimization is executed by the genetic algorithm in global scale. The effectiveness of the optimization is validated by the finite element analysis in Comsol. Compared to the traditional Halbach array with rectangle section, the magnetic field created by the proposed Halbach array in this paper owns better performance.

***doi**: 10.5829/ije.2021.34.11b.01*

**NOMENCLATURE**

| | | | |
|---|---|---|---|
| $l$ | length of one magnetic period | $N$ | total number of permanent magnets in one Halbach array |
| $\omega$ | width of each magnet segment | $n$ | the $n$th magnet segment |
| $h$ | height of the smaller magnet segment with rectangle section | $k_v$ | the linear current density of the surface current |
| $\theta$ | angle between the hypotenuse and the horizontal line in the magnet segment with trapezoid section | $\mu_0$ | the permeability of vacuum |
| $I$ | equivalent surface current | $B_{\delta_1}$ | fundamental component of the magnetic flux density |
| $B$ | magnetic flux density | $B_{r_i}$ | $i$th harmonic component |
| $K_{\mathrm{BD}}$ | sinusoidal distortion rate of the magnetic flux density | $Z$ | objective function |
| $p$ | the weighting coefficient of the $K_{\mathrm{BD}}$ | $k$ | the weighting coefficient of the $B_{\delta_1}$ |

## 1. INTRODUCTION

Klaus Halbach found a special permanent magnet array arrangement that owns stronger magnetic field on one side of the array because of the overlap and cancel out of the tangential and radial magnetic field, which is called the Halbach permanent magnet array [1]. Figure 1(a) shows the traditional regular Halbach permanent magnet array. Now, the Halbach array has been widely used in high-energy physics, high-speed motor, maglev train system, magnetic bearing and medical area [2, 3]. The ideal Halbach array is one permanent magnet whose magnetization direction varies continuously sinusoidal along the array direction, as shown in Figure 1(b). In this way, the magnetic field generated by the array can be consistent with the standard sinusoidal distribution. But due to the technical limitations and cost constraints, the ideal Halbach array cannot be manufactured.

*Corresponding Author Institutional Email: zmm2021@163.com (M. Zhu)

Please cite this article as: N. Song, M. Zhu, G. Zhou, L. Guo, Y. Mu, J. Gao, J. Ma, K. Zhang, Design and Optimization of Halbach Permanent Magnet Array with Rectangle Section and Trapezoid Section, International Journal of Engineering, Transactions B: Applications, Vol. 34, No. 11, (2021) 2379-2386

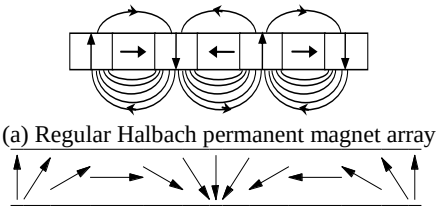

(a) Regular Halbach permanent magnet array

(b) Ideal Halbach permanent magnet array

**Figure 1.** Schematic diagram of Halbach permanent magnet array

In some occasions such as the linear motors that provide power for nanoscale positioning mechanisms, magnetic field with high performance is needed [4]. Sine there exists disparity between the magnetic field generated by traditional Halbach array and the sinusoidal, researches focused on the optimal design of permanent magnets (PM), such as unequal thickness of PM, PM with triangle section, trapezoid section or other shapes have been investigated [5-14]. Different optimization and modeling approaches were applied on the Halbach arrays' improvements. Zhang Kunlun established analytical model for linear permanent Halbach array with trapezoidal shape permanent magnets based on the theory of magnetic charge. According to kriging method, the double-sided structure motor is demonstrated to have better performance in the thrust ripple and the average thrust than single-sided structure [15]. Ren et al. [16] proposed a ring-pair permanent magnet array and the magnetic field was modeled by equivalent currents. By applying a genetic algorithm [17-19], magnetic field with high field homogeneity and high field strength was achieved [16].

A novel Halbach permanent magnet array with rectangle section and trapezoid section is presented in this paper. The surface current method is chosen to model magnetic flux density because of its closely connection with PM's configuration, which is of vital importance for optimization. The optimization method used in this paper is genetic algorithm, which is an intelligent algorithm with nonlinear, high computational efficiency and global optimization. The fundamental component of the magnetic flux density and the sinusoidal distortion rate with changeable weight coefficient compose the fitness function. Then, the better performance of the optimized Halbach array is verified by the comparison of optimized Halbach array with the traditional array and the finite element model.

## 2. STRUCTURE AND MODELING OF HALBACH ARRAY WITH RECTANGLE SECTION AND TRAPEZOID SECTION

**2. 1. Geometrical Model** As shown in Figure 2, Halbach permanent magnet array proposed in this paper is composed of magnet segments with rectangle section and trapezoid section. The dotted lines represent the beginning and ending of one magnetic period, and every five magnet segments form one magnetic period, described as $l$. There are two magnetic periods in Figure 2. The magnetization direction of magnet segments in this paper is parallel to *x* or *y* axis.

The magnet segment in the middle of one magnetic period owns bigger rectangle section. In contrast, magnet segments at the ends of one magnetic period own smaller rectangle section. Magnet segments with trapezoid section located in between the bigger and smaller magnet segments with rectangle section. Arrows on the magnet segments stand for magnetization direction, which are 90° rotated in clockwise of adjacent magnets. Residual magnetic flux density of each magnet segment is the same.

To reduce the processing costs, the width of each magnet segment is the same, expressed as $\omega$, as shown in Figure 3. The height of the smaller magnet segment with rectangle section is expressed as $h$, as shown in Figure 3(a). Figure 3(b) shows the configuration of the magnet segment with trapezoid section. The angle between the hypotenuse and the horizontal line is described as $\theta$. The height of the side, adjacent to the smaller magnet segment with rectangle section, is still $h$. According to the geometrical relationship, the height of the other side is $h+\omega\cdot\tan\theta$. In this way, the height of the bigger magnet segment with rectangle section is $h+\omega\cdot\tan\theta$.

**2. 2. Mathematical Model** In the surface current method, which is based on the Ampere's hypothesis of molecular current, the effect of the molecular electric current can be cancelled out when a permanent magnet

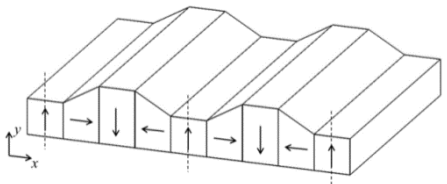

**Figure 2.** Halbach permanent magnet array with rectangle section and trapezoid section

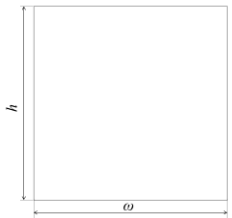

(a)Smaller magnet segment with rectangle section

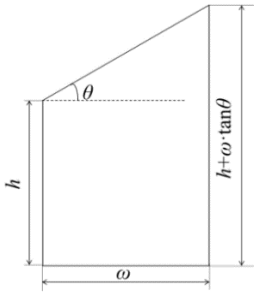


(b) Magnet segment with trapezoid section

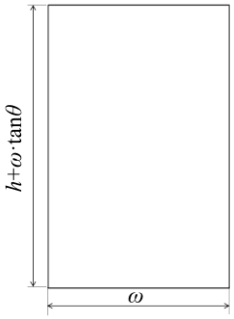


(c) Bigger magnet segment with rectangle section

**Figure 3.** Diagram of cross-section size

segment is magnetized uniformly. So, the magnetic field created by one magnet segment at any point in the outer space is equivalent to that stimulated by the surface current [20-21].

Figure 4 shows the equivalent surface current model of the smaller magnet segment with rectangle section. Coordinate system $X_1O_1Y_1$ is established in the geometric center of the cross-section, and the magnetization direction of the magnet segment shown in Figure 4 is in positive $Y$ axis. The equivalent surface currents $I_1$, $I_2$ are on the sides, and the symbols stand for the direction of currents.

According to the surface current method, the magnetic flux density stimulated by surface currents $I_1$, $I_2$ at point $\mathrm{P}(x,y)$ can be expressed as Equations (1) and (2):

$$\begin{cases} B_{I_{1x}}(x,y,k_v)=\dfrac{\mu_0 k_v}{4\pi}\ln\dfrac{\left(y+\dfrac{h}{2}\right)^2+\left(x-\dfrac{\omega}{2}\right)^2}{\left(y-\dfrac{h}{2}\right)^2+\left(x-\dfrac{\omega}{2}\right)^2} \\ B_{I_{1y}}(x,y,k_v)=\dfrac{\mu_0 k_v}{2\pi}\left(\arctan\dfrac{y-\dfrac{h}{2}}{x-\dfrac{\omega}{2}}-\arctan\dfrac{y+\dfrac{h}{2}}{x-\dfrac{\omega}{2}}\right) \end{cases} \quad (1)$$

$$\begin{cases} B_{I_{2x}}(x,y,k_v)=-\dfrac{\mu_0 k_v}{4\pi}\ln\dfrac{\left(y+\dfrac{h}{2}\right)^2+\left(x+\dfrac{\omega}{2}\right)^2}{\left(y-\dfrac{h}{2}\right)^2+\left(x+\dfrac{\omega}{2}\right)^2} \\ B_{I_{2y}}(x,y,k_v)=-\dfrac{\mu_0 k_v}{2\pi}\left(\arctan\dfrac{y-\dfrac{h}{2}}{x+\dfrac{\omega}{2}}+\arctan\dfrac{y+\dfrac{h}{2}}{x+\dfrac{\omega}{2}}\right) \end{cases} \quad (2)$$

where $k_v$ is the linear current density of the surface current.

Similarly, the equivalent surface current models of the bigger magnet segment with rectangle section and the magnet segment with trapezoid section are established, as shown in Figures 5 and 6. The coordinate system $X_2'O_2'Y_2'$ is established in the geometric center of the bigger rectangle section. The magnetization direction of the magnet segment shown in Figure 5 is in negative $Y$ axis. The equivalent surface currents $I_3$, $I_4$ are on the sides, and the symbols stand for the direction of currents, in the opposite direction compared with that in Figure 4. Based on the surface current method, the magnetic flux density stimulated by surface currents $I_3$, $I_4$ at point $\mathrm{P}'(x',y')$ in coordinate system $X_2'O_2'Y_2'$ can be expressed.

In the Halbach array, the coordinate system $X_2'O_2'Y_2'$ is $(\omega\cdot\tan\theta)/2$ away from the coordinate system

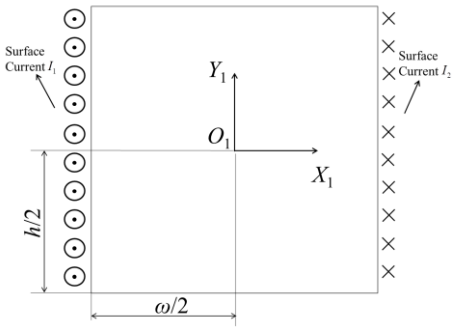


**Figure 4.** Equivalent surface current model of the smaller magnet segment with rectangle section

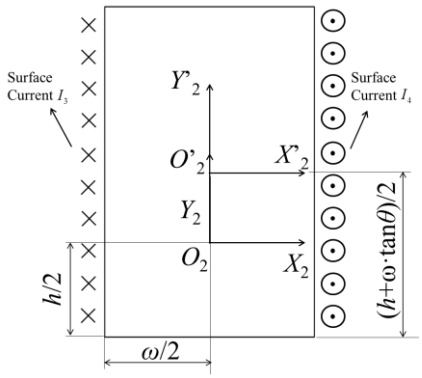


**Figure 5.** Equivalent surface current model of the bigger magnet segment with rectangle section

$X_1O_1Y_1$ on the *Y* axis, which will bring inconformity to the expression of the magnetic field at the same point away from the working face. So, coordinate system $X_2O_2Y_2$ is established by translating coordinate system $(\omega \cdot \tan\theta)/2$ downward on *Y* axis. According to the coordinate translation principle, the magnetic flux density stimulated by surface currents $I_3$, $I_4$ at point $\mathrm{P}(x, y)$ in coordinate system $X_2O_2Y_2$ can be expressed.

The coordinate system $X_3O_3Y_3$ is established in the magnet segment with trapezoid section, where the origin is located *h*/2 away from the base, $\omega/2$ away from the left side, as shown in Figure 6. The magnetization direction of the magnet segment shown in Figure 5 is in positive *X* axis. The equivalent surface current $I_5$ is on the hypotenuse, and the surface current $I_6$ is on the base. The symbols stand for the direction of currents. In the same way, the magnetic flux density stimulated by surface currents $I_6$ at point $\mathrm{P}(x, y)$ in coordinate system $X_3O_3Y_3$ can be expressed.

To describe the magnetic flux density stimulated by surface current $I_5$, coordinate system $X_3^{'}O_3^{'}Y_3^{'}$ is obtained by rotating the coordinate system $X_3O_3Y_3$ counterclockwise by an angle of $\theta$, whose coordinate axis $X_3^{'}$ is parallel to the hypotenuse. The magnetic flux density stimulated by surface current $I_5$ at point $\mathrm{P}'(x', y')$ in coordinate system $X_3^{'}O_3^{'}Y_3^{'}$ can be expressed based on the surface current method. According to the coordinate rotation theory, the magnetic flux density stimulated by surface current $I_5$ at point $\mathrm{P}(x, y)$ in coordinate system $X_3O_3Y_3$ can be expressed.

Based on the above and the superposition principle, the analytical model of the Halbach array at point can be expressed as Equation (3).

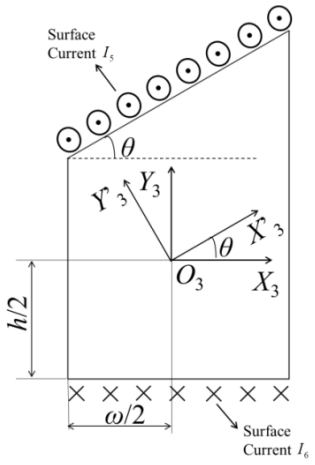


**Figure 6.** Equivalent surface current model of the magnet segment with trapezoid section

$$\begin{cases} B_x(x,y) = \sum_{n=0}^{N}\sum_{i=1}^{5} B_{ix}\left(x-\left(n+\frac{\omega}{2}\right), y, k_v\right) \\ B_y(x,y) = \sum_{n=0}^{N}\sum_{i=1}^{5} B_{iy}\left(x-\left(n+\frac{\omega}{2}\right), y, k_v\right) \end{cases} \quad (3)$$

where: *N* is the total number of permanent magnets in one Halbach array; *n* represents the *n*th magnet segment; $B_x$ is the magnetic flux density on *X* axis, $B_y$ is the magnetic flux density on *Y* axis.

## 3. OPTIMAL DESIGN OF THE HALBACH ARRAY

Based on the above, the magnetic flux density of the Halbach array is described closely related with the magnet segment's configurations, which lays a good foundation for optimization.

**3. 1. Optimization Problem** The fundamental component of the magnetic flux density $B_{\delta_1}$ indicates the magnetic energy, and the sinusoidal distortion rate $K_{\mathrm{BD}}$ can measure the sinusoid of the magnetic flux density. By executing Fourier transformation on the mathematical model of the magnetic flux density deduced from the above, harmonic components of the magnetic flux density can be obtained. $B_{\delta_1}$ is the first order of the harmonic component and $K_{\mathrm{BD}}$ can be described as:

$$K_{\mathrm{BD}} = \sqrt{\sum_{i\neq 1}\left(\frac{B_{f_i}}{B_{\delta_1}}\right)^2} \quad (4)$$

where $B_{f_i}$ is the ith harmonic component.

Both the fundamental component of the magnetic flux density and the sinusoidal distortion rate are the main performance indices of the motors. In this way, the objective function for pursuing the optimal design of motors can be defined as:

$$Z = \frac{K_{\mathrm{BD}}^{p}}{B_{\delta_1}^{k}} \quad (5)$$

where: $p$ , $k$ are the weighting coefficients. Optimization with different focus can be conducted by changing values of $p$ , $k$ .

**3. 2. Genetic Algorithm** Genetic algorithm simulates the biological genetic process. The natural selection of eliminating the poor gene is operated by the fitness evaluation on the initial group resulting from the initial coding, as shown in Figure 7. In this paper, the fitness function is expressed as Equation (5), which contains the fundamental component of the magnetic flux

density and the sinusoidal distortion rate, and the maximum fitness value is to be sought. The populations with strong magnetic flux density and low sinusoidal distortion rate are selected to produce offspring. To bring diversity to the population, crossovers and mutations are applied to the produced offspring. Then the fitness value of the evolved population is calculated and compared. The optimal solution of the objective function can be searched by evolution of multiple generations.

As one of the cases, take $l = 24mm, \omega = 6mm$ as the configuration of the traditional Halbach array, and the magnetic flux density 0.5mm away from the working face is studied. To get the Halbach array with higher performance, the angle $\theta$ and the height *h* are optimized, while other magnet segment's configurations are fixed. Considering the costs, the area of the Halbach array should be controlled, so the growth of the area is limited to 10%. It is expected that the performance of the magnetic flux density can be improved while the area decreases, so the minimum area is limited to 90% of the traditional area due to the working condition. The constraint is nonlinear because the calcualtion of the area is related with the trigonometric operation of varialbles. The angle $\theta$ is global searched in $(0,\ \pi/2)$ and the height *h* is global searched in $(4\text{mm},8\text{mm})$. In this optimization problem, $p = k = 1$ is chosen to define the objective function.

Figure 8 shows the variation of the magnetic flux density along x and y axis throughout a certain amount of iterative searches. It is obvious that the peak part of the magnetic flux density is gradually close to the trigonometric function curve, which indicates the effectiveness of the optimization. The reasonable variables that can be satisfied with strong magnetic flux density and low sinusoidal distortion rate is 9.688° and 6mm.

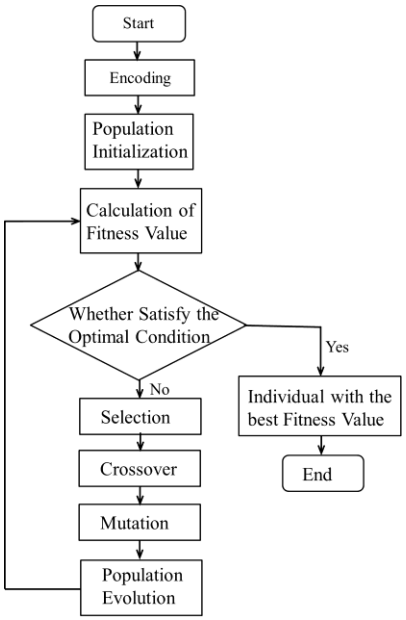


**Figure 7.** Flowchart of the GA

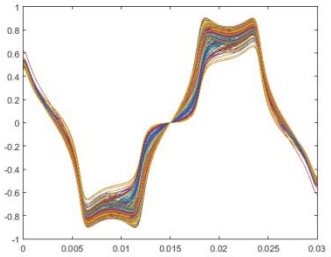

(a) *x* axis

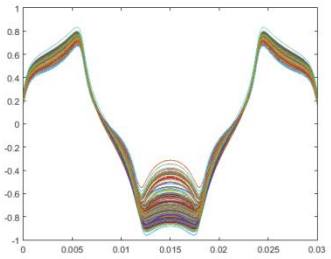

(b) *y* axis

**Figure 8.** Variation of the magnetic flux density

## 4. RESULT AND DISCUSSION

The parameters of the optimized Halbach permanent magnet array are listed in Table 1, and the structure diagram of the optimized Halbach permanent magnet array in one magnetic period is shown in Figure 9. The traditional Halbach permanent magnet array composed of smaller magnet segment with rectangle section is proposed for comparison, as shown in Figure 10. According to calculation, the area of the traditonal Halbach array is $1.8\times10^{-4}\,\text{m}^2$ and the optimized is $1.92\times10^{-4}\,\text{m}^2$.

Comparing the magnetic flux density 0.5mm away from the working face generated by the optimized array in Figure 9 and those of the traditional array in Figure 10, the optimized magnet array has the sinusoidal distortion rate $K_{\text{BD}}$ of 0.1813 and the fundamental component of

**TABLE 1.** Parameters of Halbach array

| **Parameters** | **Fixed** | | | **Variable** | |
|---|---|---|---|---|---|
| | Magnetic Period/ (*l*) | Width ($\omega$) | Residual Magnetism ($B_r$) | Angle ($\theta$) | Height (*h*) |
| Value | 24 mm | 6 mm | 1.35T | 9.688° | 6mm |

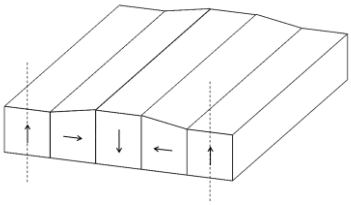

**Figure 9.** Schematic diagram of the specific Halbach permanent magnet array

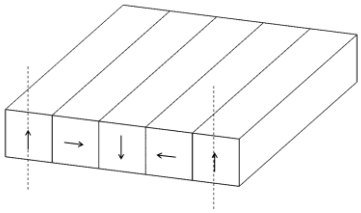

**Figure 10.** Schematic diagram of the traditional Halbach permanent magnet array

the magnetic flux density of 0.9672T, whereas the traditional magnet array has the sinusoidal distortion rate $K_{\mathrm{BD}}$ of 0.2057 and the fundamental component of the magnetic flux density of 0.9772T. As can be seen, the optimization reduces the sinusoidal distortion rate by 11.86% with a sacrifice of the field strength of 1.02% and the area of 6.82%. The optimization offers significant improvement in sinusoidal while still maintains a similar field strength. Also, the added cost can be beared. The solid lines represent the magnetic flux density of the optimized magnet array along *x* and *y* axis in Figure 11, and the dotted lines represent those of the traditional array. Specific value of the main performance indices are shown in Table 2.

In order to verify the feasibility of the modeling method, the magnetic flux density 0.5mm away from the working face generated by the optimized array are evaluated by the finite element model. The dotted line in Figure 12 represents the magnetic flux density in finite element method and the solid line represents the

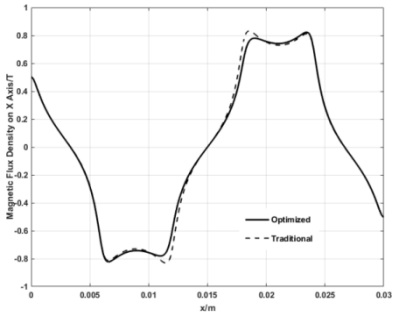


(a) *x* axis

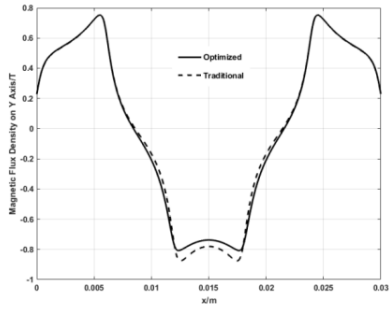


(b) *y* axis

**Figure 11.** Comparison of the magnetic flux density of the optimized and traditional magnet array

**TABLE 2.** Comparison of the Evaluation Indexes of Halbach Magnet Arrays

| Index | Type | |
|---|---|---|
| | **Traditional** | **Optimized** |
| $B_{\delta_{1x}}$ (T) | 0.6481 | 0.6412 |
| $B_{\delta_{1y}}$ (T) | 0.7313 | 0.7241 |
| $B_{\delta_1}$ (T) | 0.9772 | 0.9672 |
| $K_{\mathrm{BDx}}$ | 0.1629 | 0.1411 |
| $K_{\mathrm{BDy}}$ | 0.1256 | 0.1138 |
| $K_{\mathrm{BD}}$ | 0.2057 | 0.1813 |
| Area | $1.8\times10^{-4}\mathrm{m}^2$ | $1.92\times10^{-4}\mathrm{m}^2$ |

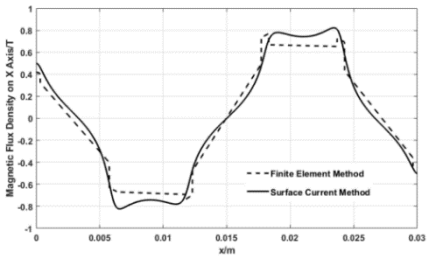


(a) *x* axis

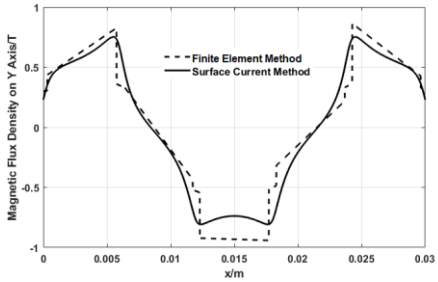


(b) *y* axis

**Figure 12.** Comparison of the magnetic flux density of surface current method and finite element method

magnetic flux density by the surface current method. It can be seen that lines follow the same trend and the magnetic flux density described by the surface current method contain more details.

## 5. CONCLUSION

The design and optimization of a novel Halbach permanent magnet array with rectangle section and trapezoid section is proposed. The magnetic flux density of the array is modeled according to the surface current method, which is closely related with the magnet segment's configurations. The feasibility of the modeling method is validated in the finite element method. To achieve better magnetic flux density performance, the genetic algorithm is applied based on the above. As the main performance indices, the fundamental component of the magnetic flux density and the sinusoidal distortion rate are chosen to construct the fitness function. Compared with the traditional Halbach array, the optimized Halbach array owns significant improvement in sinusoidal while still maintains similar field strength.

## 6. ACKNOWLEDGMENTS

This work was supported by the Natural Science Foundation of Shandong Province (Grant No. ZR2019BEE038), the Youth Foundation of Shandong Academy of Sciences (2020QN0031), the Collaborative Innovation Fund of Shandong Academy of Sciences (2019CXY25), the Major Science and Technology Innovation Project of Shandong Province (2019JZZY010912), and the Special Construction Project of Engineering Technology Research Center of Shandong Province (2019JZP014).

## 7. REFERENCES

1. Halbach K., "Design of permanent multipole magnets with oriented rare earth cobalt materials" ***Nuclear Instruments and Methods***, Vol. 169, No. 1, (1980), 1-10. doi.org/10.1016/0029-554X(80)90094-4
2. Zhang L., Kou B., Xing F., Jin Y., Zhang H., Zhu J., "Magnetically levitated synchronous permanent magnet planar motor with concentric structure winding used for lithography machine" ***Journal of Applied Physics***, Vol. 11, No. 7, (2015), 15-25. doi.org/10.1063/1.4917332
3. Zhu H., Pang C. K., Teo T. J., "Analysis and control of a 6 DOF maglev positioning system with characteristics of end-effects and eddy current damping" ***Mechatronics***, Vol. 47, (2017), 183-194. doi.org/10.1016/j.mechatronics.2016.12.004
4. Song N. R., Ma S.Y., Zhang Z.Q., "A numerical study of forces for sandwiched maglev stage", ***International Journal of Applied Electromagnetics and Mechanics***, Vol. 55, (2017), 89-100. DOI: 10.3233/JAE-160152
5. Fang, S. H., Xue, S. H., Pan, Z. B., et al. "Torque ripple optimization of a novel cylindrical arc permanent magnet synchronous motor used in a large telescope", ***Energies***, Vol. 12, (2019), 362-377. doi.org/10.3390/en12030362
6. Li Z. J., Yan Z. J., Luo J. T., "Performance comparison of electromagnetic energy harvesters based on magnet arrays of alternating polarity and configuration", ***Energy Conversion and Management***, Vol. 179, (2019), 132-140. doi.org/10.1016/j.enconman.2018.10.060
7. Arish N., Teymoori V., "Development of Linear Vernier Hybrid Permanent Magnet Machine for Wave Energy Converter", ***International Journal of Engineering, Transactions B: Applications***, Vol. 33, No. 5, (2020), 805-813. DOI: 10.5829/IJE.2020.33.05B.12
8. Arish N., Marignetti F., "Evaluation of Linear Permanent Magnet Vernier Machine Topologies for Wave Energy Converters", ***International Journal of Engineering, Transactions B: Applications***, Vol. 34, No. 2, (2021), 403-413. DOI: 10.5829/IJE.2021.34.02B.12
9. Uberruck T., Blumich B., "Variable magnet arrays to passively shim compact permanent-yoke magnets", ***Journal of Magnetic Resonance***, Vol. 298, (2019), 77-84. doi.org/10.1016/j.jmr.2018.11.011
10. Zhang Y., Cao J. Y., Zhu H. Y., "Design, modeling and experimental verification of circular Halbach electromagnetic energy harvesting from bearing motion", ***Energy Conversion and Management***, Vol. 180, (2019), 811-821. doi.org/10.1016/j.enconman.2018.11.037
11. Meribout M., Sonowan S., "Optimal Halbach magnet array design for portable NMR targeting multiphase flow metering applications", ***IEEE Transactions on Magnetics***, Vol. 1, No. 55, (2019). DOI: 10.1109/TMAG.2018.2877603
12. Zhang Y. Q., Yu M.H., "Field and thrust analysis of linear servo motor with permanent-magnet of different shapes", in Proceedings of IEEE ICEM conference, Kuala Lumpur, Malaysia, (2010), 1516-1519.
13. Zhang Y. Q., Yu M.H., "Analysis and design of double-sided air core linear servo motor with trapezoidal permanent magnets", ***IEEE Transactions on Magnetics***, Vol. 47, No. 10, (2011), 3236–3239. DOI: 10.1109/TMAG.2011.2156398
14. Meessen K. J., Gysen B. L., "Halbach permanent magnet shape selection for slotless tubular actuators", ***IEEE Transactions on Magnetics***, Vol. 44, No. 11, (2008), 4305-4308. **DOI:** 10.1109/TMAG.2008.2001536
15. Duan J. H., Xiao S., Zhang K. L., Jing Y.Z., "A novel 3-D analytical modeling method of trapezoidal shape permanent magnet Halbach array for multi-objective optimization", ***Journal of Electrical Engineering & Technology***, Vol. 14, (2019), 635-643.
16. Ren Z. H., Mu W. C., Huang S. Y., "Design and optimization of a ring-pair permanent magnet array for head imaging in a low-field portable MRI system", ***IEEE Transactions on Magnetics***, Vol. 1, No. 55, (2019) 1-8. DOI: 10.1109/TMAG.2018.2876679
17. S. Mohammadi, M. Babagoli. "A Hybrid Modified Grasshopper Optimization Algorithm and Genetic Algorithm to Detect and Prevent DDoS Attacks". ***International Journal of Engineering, Transactions A: Basics***, Vol. 34, No. 4, (2021), 811-824. doi.org/10.5829/ije.2021.34.04a.07
18. L. Izadi, F. Ahmadizar, J. Arkat. "A Hybrid Genetic Algorithm for Integrated Production and Distribution Scheduling Problem with Outsourcing Allowed". ***International Journal of Engineering, Transactions B: Applications***, Vol. 33, No. 11, (2020), 2285-2298. DOI: 10.5829/IJE.2020.33.11B.19
19. M. Parvane, E. Rahimi, F. Jafarinejad. "Optimization of Quantum Cellular Automata Circuits by Genetic Algorithm". ***International Journal of Engineering, Transactions B:***

***Applications***, Vol. 33, No. 2, (2020), 229-236. doi.org/10.5829/ije.2020.33.02b.07

20. Luo C., Zhang K. L., Zhang W. L., Jing Y. Z., "3D analytical model of permanent magnet and electromagnetic hybrid Halbach array electrodynamic suspension system", ***Journal of Electrical Engineering & Technology***, Vol. 15, (2020), 1713-1721.
21. Luo C., Zhang K. L., Zhang W. L., Jing Y. Z., "Study of permanent magnet electrodynamic suspension system with a novel Halbach Array", ***Journal of Electrical Engineering & Technology***, Vol. 15, (2020), 969-977.

## Persian Abstract

**چکیده**

در این مقاله ، یک آرایه آهنربای دائمی Halbach با بخش مستطیل و بخش ذوزنقه ای پیشنهاد و بهینه شده است. مدل تحلیلی آرایه Halbach بر اساس روش جریان سطحی ایجاد شده است ، که از لحاظ عددی کارآمد است و می تواند برای ارزیابی میدان مغناطیسی آرایه Halbach ناشی از تنظیمات مختلف بخش آهنربایی مورد استفاده قرار گیرد. جزء اساسی چگالی شار مغناطیسی و میزان اعوجاج سینوسی به عنوان شیء بهینه سازی انتخاب شده و بهینه سازی توسط الگوریتم ژنتیک در مقیاس جهانی اجرا می شود. اثربخشی بهینه سازی با تجزیه و تحلیل اجزای محدود در Comsol تأیید می شود. در مقایسه با آرایه سنتی Halbach با بخش مستطیل ، میدان مغناطیسی ایجاد شده توسط آرایه Halbach پیشنهادی در این مقاله دارای عملکرد بهتری است.